



Diminished MYCN Dosage Endows Cavitory Transformation in Retinoblastoma

Mingpeng Xu, MD,^{1,*} Hanhan Shi, MD, PhD,^{2,3,*} Yongning Shen, BS,^{2,3,*} Ludi Yang, MD,^{2,3,*} Yu Luan, MD,^{2,3} Xiang Gu, MD,^{2,3} Xuyang Wen, MD, PhD,^{2,3} Chuandi Zhou, MD, PhD,^{2,3} Renbing Jia, MD, PhD,³ Xunda Ji, MD, PhD,¹ Peiquan Zhao, MD, PhD,¹ Minglei Han, MD, PhD,^{2,3} Jiayan Fan, MD, PhD,^{2,3} Peiwei Chai, MD, PhD^{2,3}

Objective: Cavitory retinoblastoma (CRB) represents a unique variant of retinoblastoma (RB) distinguished by the presence of translucent cavities, which are discernible through ophthalmoscopic examination. The present study was designed to elucidate the clinical implications and molecular signatures of CRB, thereby enhancing our understanding of this distinct subtype of RB.

Design: A multicentric, nested case-control, retrospective cohort study combining spatial proteomic analysis.

Participants: In a longitudinal study encompassing 1360 RB patients, conducted over a 13-year timeframe from June 2008 to February 2022, cavitory spaces were detected within the tumors of 48 eyes of 46 patients. A control cohort of 180 eyes from 138 age-matched patients with non-CRB was selected, maintaining a 1:3 case-control ratio. Laser-captured spatial proteomic analysis was conducted to explore the pivotal molecular changes within this specific subtype. The silencing of MYCN was achieved using adeno-associated virus (AAV) 2-mediated gene therapy in patient-derived xenograft models.

Intervention: Enucleation, chemotherapy, and focal therapy.

Main Outcome Measures: Overall survival and metastasis-free survival.

Results: Cavitory RB was linked to enhanced metastasis-free survival ($P = 0.007$) and overall survival ($P = 0.03$), as well as an increased proportion of well-differentiated status ($P < 0.001$) and a reduced incidence of vitreous seeding ($P = 0.02$). Spatial proteomic analysis, immunofluorescence, and immunohistopathology revealed a lower MYCN expression in CRB than in non-CRB. Silencing MYCN in patient-derived xenografts using AAV recapitulated these phenotypes of CRB, including the formation of translucent cavities and the emergence of cone-like rosettes.

Conclusions: This study establishes a novel genetic–phenotypic association, revealing that diminished MYCN expression induces the formation of translucent cavities. This phenotype is indicative of a less aggressive, well-differentiated CRB subtype with a more favorable prognosis.

Financial Disclosure(s): The author(s) have no proprietary or commercial interest in any materials discussed in this article. *Ophthalmology Science* 2025;5:100820 © 2025 by the American Academy of Ophthalmology. This is an open access article under the CC BY-NC-ND license (<http://creativecommons.org/licenses/by-nc-nd/4.0/>).



Supplemental material available at www.opthalmologyscience.org.

Retinoblastoma (RB), a significant and potentially fatal intraocular malignancy in children, necessitates identification of its characteristic ophthalmoscopic attributes for diagnosis.¹ The typical presentation of RB involves the emergence of a solid yellow–white mass from the retina, frequently accompanied by additional indicators such as dilated tortuous vessels, subretinal fluid, subretinal seeds, and vitreous seeds.² Clinically observable calcification regions manifest as white clumps resembling cottage cheese. The majority of clinicians rely on these features to diagnose RB.³

Infrequently, cavitory RB (CRB) may exhibit ophthalmoscopically visible lucent cavities.⁴ These cavities manifest as hollow spaces on ultrasonography and display hypofluorescence on angiography.⁵ Retinoblastoma commonly exhibits a good response to chemotherapy,

leading to the resolution of retinal detachment and tumor shrinkage.⁶ However, prior studies on CRB have indicated its inherent chemoresistant and radioresistant characteristics. Even though the reduction in tumor size is not significant, there is a tendency for them not to relapse and perhaps display a more favorable prognosis.^{7,8} Currently, adjuvant therapies, such as consolidation laser treatment in conjunction with chemotherapy, are being employed for the treatment of RB. Notably, laser has to be carefully used in CRB due to the risk of cyst rupture and eventual vitreous seeding. For its relatively quiescent phenotypes, it has been proposed that extended adjuvant therapy is not required in cases of complete response to treatment.⁹

Histopathologically, the cavitory spaces within RB were found to correspond to regions of photoreceptor differentiation that are in close proximity to the cavitations.⁴ This

distinctive characteristic might account for the observed phenomenon of a subdued therapeutic response and a comparatively lower propensity for tumor reactivation. However, only very limited histopathological reports have mentioned the presence of cavitory spaces in RB. Moreover, the clinical significance of this finding has been primarily explored within the context of case-series studies, which are inherently constrained by their limited sample sizes. Most importantly, the molecular basis of the formation of CRB is unknown.

Methods

Ethical Approval

This study adhered to the tenets of the Declaration of Helsinki. A centralized institutional review board review process was used in this study. This study was approved by the institutional review board of the lead unit, Shanghai Ninth People's Hospital, Shanghai Jiao Tong University School of Medicine (2017-353-T262, SH9H-2019-T185-2). Written informed consent was obtained from each patient's parents. Human tumor specimens were obtained from patients who had undergone surgical eye removal. Participation in this study was voluntary for all patients, with no additional compensation provided.

The animal studies were granted approval by the Animal Ethics Committee of Shanghai Jiao Tong University School of Medicine, with reference number SH9H-2021-A058-SB, and were conducted in strict adherence to the prevailing institutional and international standards for the welfare and utilization of animals. BALB/c nude mice, aged 4 weeks, were procured from Slack Company and were housed in the hospital's specific pathogen-free Laboratory Animal Facility.

Participants and Follow-Up

A centralized institutional review board review process was used in this multicenter study. Consecutive patients who were diagnosed with RB from June 2008 through February 2022 were included and managed at the Ocular Oncology Service at Shanghai Ninth People's Hospital, Shanghai Xinhua Hospital, and Shandong Qilu Children's Hospital. The exclusion criteria were as follows: (1) low quality of fundus photography or medical imaging; (2) unable to distinguish cavitory status or extraocular cases; (3) had evidence of other malignancy at the onset of presentation or trilateral cases; and (4) refused regular follow-up and recommended therapy. Finally, this study included 1154 patients who were eligible for final analysis. Among these cases, 46 tumors with clinically visible cavitory spaces were selected for further study. A representative clinical presentation of CRB is illustrated in Figure 1A–D. Age-matched children with noncavitory subtype RB were also included in a case-control ratio of 1:3 (scans were acquired from June 2008 to February 2022, and data were collected from May 2010 to October 2020, with a caliper width of ± 0.5 years). The mean follow-up period was 61.84 ± 33.72 months. The enrollment and follow-up details are depicted in Figure S1 (available at www.opthalmologyscience.org).

In this study, a record was maintained for each patient, documenting the age at diagnosis in months, sex, and the initial presenting sign, which included leukocoria, strabismus, and poor vision. The RB's laterality was assessed, distinguishing between unilateral and bilateral. Each affected eye was classified using the international intraocular RB classification criteria to standardize the evaluation.¹⁰ The intravenous chemotherapy (IVC) protocol

followed a standard regimen of 6 cycles, administered at intervals of 3 to 4 weeks, comprising vincristine, etoposide, and carboplatin across all institutions. Intra-arterial chemotherapy was delivered in 3 to 4 cycles, utilizing a 2- or 3-drug combination from a panel that included melphalan, topotecan, and carboplatin, following previous protocols.³ The synergistic approach involved an initial phase of 2 to 3 rounds of IVC, followed by a subsequent phase of 2 to 3 rounds of intra-arterial chemotherapy. Chemotherapy response grading was assessed by RECIST 1.1 criteria.¹¹

Focal treatments were also employed, primarily consisting of photocoagulation, cryotherapy, and brachytherapy. Laser photocoagulation and cryotherapy were selectively applied to tumors measuring < 3 mm, particularly new tumors. Laser photocoagulation was the preferred modality for posterior retinal tumors, while cryotherapy was reserved for peripheral lesions, particularly those near the ora serrata. Throughout the treatment period, patients underwent monthly fundus photography under anesthesia to facilitate evaluation and inform decisions regarding subsequent therapeutic interventions. Enucleation was reserved for cases with the following indications: fundus hemorrhage, neovascular glaucoma, signs of optic nerve involvement, or evidence of extraocular disease on imaging, as well as for phthisis bulbi, uncontrollable seeds, or tumor recurrence.

The flow chart of the analysis of enucleated tumors is depicted in Figure S2 (available at www.opthalmologyscience.org). Histopathology was performed for enucleated eyes, and the cavitory variant was further validated by the pathological examination. The assessment of tumor differentiation was conducted by scrutinizing all viable regions of the tumor. The tumor was categorized as undifferentiated in the absence of any Flexner–Wintersteiner or Homer–Wright rosettes.⁹ It was deemed poorly differentiated when such rosettes were observed in < 2 focal spots. A diagnosis of moderate differentiation was given when rosettes were evident in > 2 areas, yet not uniformly distributed across the majority of the viable tumor regions. Conversely, a tumor was classified as well differentiated when rosettes were a dominant feature throughout most of the viable tumor areas. Furthermore, all cases were reevaluated by pathologists, who applied the classification criteria outlined in the eighth edition of the American Joint Committee on Cancer for comparative analysis.¹² This process ensured a standardized and updated assessment of tumor differentiation in line with contemporary oncological standards. The vital status of the patients was verified through the mandatory Chinese resident registry and the data recorded by the Chinese Center for Disease Control, leveraging the national identification number for accuracy and reliability.

Tissue Processing for Laser-Capturing Microdissection

Formalin-fixed paraffin-embedded tissue sections of CRB and non-CRB were cut ($8 \mu\text{m}$), collected, air dried, and heated at 65°C for 60 minutes to facilitate better adhesion. Next, sections were deparaffinized, rehydrated, and loaded wet as follows: 2×2 min xylene, 2×1 min 100% ethanol (EtOH), 95% EtOH, 85% EtOH, 75% EtOH, 50% EtOH, and ddH₂O, respectively. The tissue sections then were stained with hematoxylin and eosin as follows. Each slide was processed with hematoxylin, bluing buffer, and eosin for 7 minutes, 2 minutes, and 40 seconds, respectively. And the residual buffer used in the last step was washed with water.

Laser-capture microdissection (LCM) procedure was completed on Laser-Capture Microdissection System PALM (Zeiss), as previously described.^{13,14} The LCM system was turned and kept on

MRI-T2

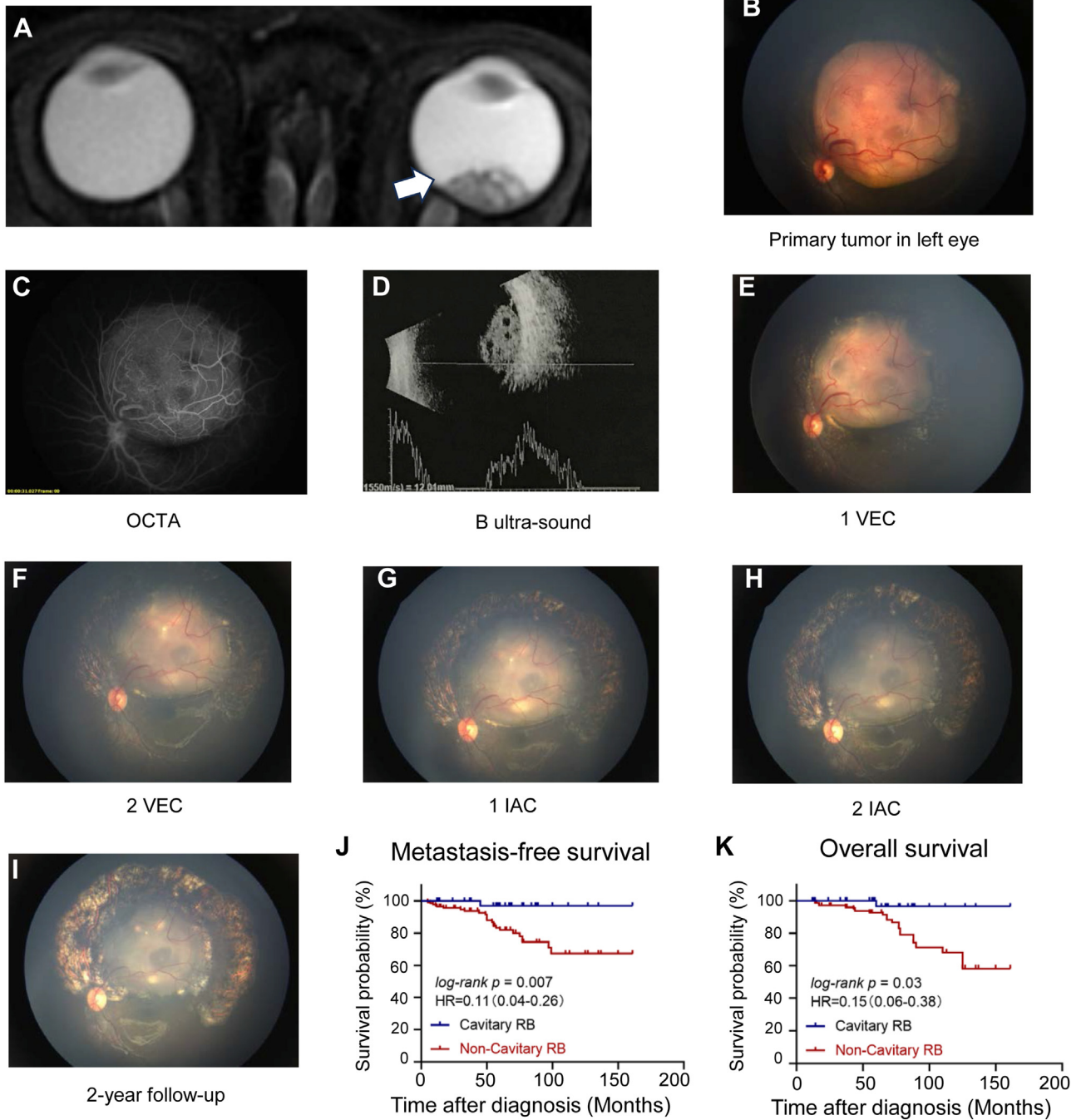


Figure 1. Characterization of cavitory retinoblastomas in terms of clinical manifestations, chemotherapy response, and prognostic outlook. **A**, High-resolution T2-weighted MRI displays pronounced high-signal intensities within the tumor’s cavities, indicated by the white arrow. **B**, **C**, Tumor surface analysis through fundus photography (**B**) and OCTA (**C**) reveals the presence of multiple translucent cavities, clearly visible on the tumor’s surface. **D**, Ultrasonography (B-mode ultrasound) depicts the presence of multiple hollow spaces within the tumor, as indicated by the imaging technique. **E** to **I**, A series of illustrations depict the chemotherapy response observed with the combined approach of intravenous chemotherapy and IAC administration. **J** and **K**, Kaplan–Meier survival analysis demonstrates a significant advantage in survival outcomes for patients with cavitory retinoblastomas compared with those with noncavitory tumors, as evidenced by both MFS (**J**) and OS (**K**) metrics. HR = hazard ratio; IAC = intra-arterial chemotherapy; MFS = metastasis-free survival; MRI = magnetic resonance imaging; OCTA = OCT angiography; OS = overall survival; RB = retinoblastoma; VEC = etoposide, epirubicin, cisplatin.

for 15 minutes to stabilize the laser energy. Microscope and laser settings were settled upon as follows: Zoom: 20×; cut energy: 39; focus: 62; catapulting energy: 64; focus: 70; cycle number:

1; cut speed: 100. The dried-hematoxylin and eosin-stained slide was put onto the slide adapter of the LCM microscope. The regions of interest containing a specific cell type in the section were

marked with an LCM marker pen and microdissected using the above-mentioned settings and collected with microtubes (Zeiss, 415190-9201-000). The microdissected samples were stored at -80°C or digested for proteomic analysis.

Sample Preparation and Mass Spectrometer

The microdissected samples were resuspended with 5 μL lysis buffer and were sonicated for 3 minutes using a contactless high-intensity ultrasonic processor (Scientz) and then were incubated at 95°C for 5 minutes. Protein digestion was performed overnight at 37°C after adding 1 μL of 50 ng trypsin. The peptides were desalted using C18 ZipTips according to the manufacturer's instructions and then dried for further mass spectrum (MS) analysis. The separated peptides were analyzed in Orbitrap Astral with a nano-electrospray ion source. The electrospray voltage applied was 1900 V. Precursors were analyzed at the Orbitrap detector, and the fragments were analyzed at the Astral detector. The full MS scan resolution was set to 240 000 for a scan range of 400 to 800 m/z . The MS/MS scan was fixed first mass as 150.0 m/z at a resolution of 80 000. The high energy collision dissociation fragmentation was performed at a normalized collision energy of 25%. The automatic gain control target was set at 800%, with a maximum injection time of 15 ms.

Immunohistopathology and Immunofluorescence

Immunohistopathology and immunofluorescence staining methods were described previously.^{15,16} Intensity of MYCN expression was scored in the immunohistopathology as follows: level 0 = negative, level 1 = low, level 2 = medium, and level 3 = high. The extent of MYCN expression was quantified as the percentage of positively stained cells observed relative to the entire tumor area with a score of 0 for $<1\%$, 1 for 2% to 10%, 2 for 11% to 50%, 3 for 51% to 75%, and 4 for $>75\%$. For immunofluorescence analysis, the samples were first incubated with primary antibodies at 4°C overnight, followed by incubation with corresponding secondary antibodies for 1 hour at room temperature. The nuclei were then stained with 4',6-diamidino-2-phenylindole (Sigma-Aldrich) for 30 minutes at room temperature. Fluorescent images were captured using an OLYMPUS microscope (Olympus Co). The samples were treated with a rabbit anti-MYCN monoclonal antibody (1:200 dilution, catalog number ab227822, Abcam). To enumerate positive cells, 4 distinct microscopic fields within each tumor section were examined. The optical density of the positive staining in each image was quantified using ImageJ software version 1.52. Relative MYCN expression levels were ascertained by comparing the fluorescence intensity of the target antibody to that of the 4',6-diamidino-2-phenylindole-stained nuclei.

Patient-Derived Orthotopic Xenograft Model Experiments

A total of 4×10^5 cells for the patient-derived xenograft model were implanted on the retinas through subretinal injection to establish a stable orthotopic RB model in BALB/c nude mice (male, 4–5 weeks old), as previously described.¹⁷ The eyeball volume was calculated by the formula $\text{volume} = \text{length (mm)} \times \text{width (mm)}^2/2$. The eyeballs of each mouse were measured every 7 days for 28 consecutive days.

The Production and the Delivery of Adeno-Associated Virus and Efficacy Validation

Recombinant adeno-associated virus (AAV)-shMYCN was packaged by PackGene BioTech as previously described.¹⁸ Especially, AAV-shMYCN was cloned and inserted into the AAV plasmid containing the U6 promoter, with a viral titer of 3.95×10^{12} vg/ml. All AAV serotype vectors were produced in HEK 293T cells cotransfected with the rep-cap fused plasmid and a helper plasmid. Adeno-associated viruses were purified by iodixanol gradient ultracentrifugation. The AAV-carrying shMYCN sequence is 5'-GCCAGTATTAGACTGGAAGTT-3', as previously described.¹⁹ The control sequence of shMYCN is 5'-CCTAAGGTTAAGTCGCCCTCGC-3'. The eyeballs of each mouse were measured every 7 days for 28 consecutive days.

The patient-derived xenograft animals were randomly allocated into 2 groups: one receiving AAV2-shMYCN and the other receiving an empty vector. Intravitreal injections were administered using a micropipette, carefully inserted behind the superotemporal limbus through the sclera into the vitreous cavity. A volume of 1 μL of viral particles was delivered into the vitreous cavity, as previously described.²⁰ The silencing efficacy was determined by quantitative reverse transcription polymerase chain reaction, western blot (MYCN antibody: Abcam, ab227822; β -actin antibody: Abcam, ab8226), and immunofluorescence analysis (MYCN antibody: Abcam, ab227822).

Statistical Analysis

The statistical analyses were conducted utilizing IBM SPSS Statistics version 24.0 (SPSS, Inc) and R software version 3.4.1 (R Foundation for Statistical Computing). Categorical variables were described using counts (percentages), while continuous variables were summarized with medians (interquartile ranges). To compare medians and proportions, we employed the nonparametric Mann–Whitney U test and the chi-square test, with the Fisher exact test used where appropriate. Kaplan–Meier survival analysis was implemented to estimate overall survival and metastasis-free survival, and the log-rank test was utilized to assess the differences in survival among subgroups. For patients who were still alive at the conclusion of the follow-up period, their data were treated as censored. The hazard ratios along with their 95% confidence intervals were computed. Quantification data are presented as the mean \pm standard deviation, and the differences between 2 groups were compared by unpaired Student t test. All statistical tests were conducted as 2-sided, and a P value of <0.05 was deemed to indicate statistical significance.

Results

Descriptive Statistics

In a 13-year longitudinal study encompassing 1154 RB patients from 3 tertiary RB centers, cavitory spaces within RBs were ophthalmoscopically detected in 48 eyes of 46 patients, which corresponds to an incidence rate of 4.0%. The mean age at diagnosis for CRB was 17.2 months, with a sex ratio of 25 males to 21 females. Of the CRB patients, 21.7% (10/46) had bilateral RB, while only 2 cases (4.3%) featured bilateral CRB (Table 1).

Clinical presentations are delineated in Table 2. The majority of CRB patients were diagnosed at group D, accounting for 58.3% (28/48) of the cases, with 18.8% (9/48) at stage E and 20.8% (10/48) at stage C. The most

Table 1. Demographic and Clinical Characteristics for Patients with Cavitory Retinoblastoma and Noncavitory Controls

Number of Patients	Cavitory RB (n = 46)	Noncavitory RB (n = 138)	P
Age at onset (mos ± SEM)	17.22 ± 1.23	16.79 ± 1.07	0.83
Follow-up mos (mos ± SEM)	62.46 ± 4.58	61.15 ± 2.95	0.82
Sex			
Male	25 (54.3)	74 (53.6)	0.73
Female	21 (45.7)	64 (46.4)	
Laterality			0.26
Unilateral	36 (78.3)	96 (69.6)	
Bilateral	10 (21.7)	42 (30.4)	
Secondary malignancy			1.00
Present	0 (0.0)	2 (1.4)	
Absent	46 (100.0)	136 (98.6)	
Treatment			
Intravenous chemotherapy	25 (54.3)	72 (52.2)	0.80
Intra-arterial chemotherapy	20 (43.5)	67 (48.6)	0.55
Intravitreal chemotherapy	8 (17.4)	20 (14.5)	0.64
Periocular chemotherapy	1 (2.2)	6 (4.3)	0.68
Vitreotomy	1 (2.2)	2 (1.4)	1.00
Laser photocoagulation	11 (23.9)	32 (23.2)	0.92
Cryotherapy	10 (21.7)	34 (24.6)	0.70
Primary enucleation	8 (17.4)	21 (15.2)	0.73
Secondary enucleation	2 (4.3)	17 (12.3)	0.16
Outcome			
Metastasis	1 (2.2)	24 (17.4)	0.009*
Death	1 (2.2)	22 (15.9)	0.015*

RB = retinoblastoma; SEM = standard error of the mean.

Data are presented as number (%).

* $P < 0.05$.

prevalent initial symptom was leukocoria, affecting 85.4% (41/48) of the patients, followed by strabismus at 12.5% (6/48) and proptosis (10.4%, 5/48).

A comparative analysis was conducted with a 1:3 case-controlled ratio of noncavitory group, comprising 138 age-matched individuals with 180 noncavitory tumors. No significant differences were observed in the parameters examined, such as the age of onset ($P = 0.83$), sex ($P = 0.73$), and laterality ($P = 0.26$) between the CRB and non-CRB groups. A significantly lower incidence of vitreous seeds was noted in the CRB group ($P = 0.02$) compared with the non-CRB group, which is agreeable with previous observations.⁴ Despite this, other clinical and pathological features did not exhibit significant variations between the 2 groups. This includes the prevalence of leukocoria ($P = 0.90$), strabismus ($P = 0.66$), proptosis ($P = 0.56$), orbital cellulitis ($P = 0.08$), optic nerve thickening ($P = 0.38$), choroidal invasion ($P = 0.28$), optic nerve invasion ($P = 0.14$), iris neovascularization ($P = 0.09$), and intraocular RB classification tumor staging.

Chemotherapy Responses and Outcome

The treatment-related variables for the study are outlined in [Table S1](#) (available at www.ophtalmologyscience.org). Among the 37 CRB tumors treated with chemotherapy, 17 patients underwent IVC (IVC), and 12 were treated with intra-arterial chemotherapy. Additionally, a synergistic therapeutic strategy combining both intra-arterial chemotherapy and IVC was employed for all 8 patients.

It is of particular interest to note that the IVC group demonstrated a comparatively lower complete response rate to chemotherapy, with a success rate of 70.6%, translating to 12 of 17 patients. In contrast, the group that received the combined treatment of intra-arterial chemotherapy and IVC achieved a remarkable complete response rate of all 8 patients (100.0%). One typical case of CRB is described in [Figure 1E–I](#). It is also important to highlight that no significant disparities in chemotherapy response were observed between the CRB and non-CRB groups.

In terms of surgical interventions, enucleation was carried out in 10 CRB patients; this included 8 cases of primary enucleation and 2 cases of secondary enucleation due to tumor recurrence and vitreous hemorrhage, respectively. All tumors were cavitory variants, as evidenced by the presence of translucent cavities in the histopathologic examination. A thorough review of the pathology results from the enucleated eyes revealed that 90% of the tumors (9/10) were well-differentiated, with extensive regions of photoreceptor differentiation, and no viable tumor cells were present at the edges of the cavities. The proportion of well-differentiated tumors is significantly higher than the non-CRB group ($P < 0.001$, [Table 2](#)). These findings are consistent with previous observations.^{4,7,21}

During the follow-up time (median: 62.5 months for the CRB group, 61.2 months for the non-CRB group), only 1 intracranial metastasis and death is observed in CRB group. In contrast, 24 metastases (17.4%) and 22 deaths (15.9%) are observed in the non-CRB group ([Table 1](#)). By

Table 2. Ocular Symptoms in Patients with Cavitory Retinoblastoma and Noncavitory Controls

Total Eyes	Cavitory RB (n = 48)*	Noncavitory RB (n = 180)	P
Leukocoria			0.90
Present	41 (85.4)	155 (86.1)	
Absent	7 (14.6)	25 (13.9)	
Strabismus			0.66
Present	6 (12.5)	27 (15.0)	
Absent	42 (87.5)	153 (85.0)	
Proptosis			0.56
Present	5 (10.4)	14 (7.8)	
Absent	43 (89.6)	166 (92.2)	
Orbital cellulitis			0.08
Present	0 (0.0)	13 (7.2)	
Absent	48 (100.0)	167 (92.8)	
Optic nerve thickening [†]			0.38
Present	2 (4.2)	17 (9.4)	
Absent	46 (95.8)	163 (90.6)	
Vitreous seeding			0.02 [§]
Present	2 (4.2)	33 (18.3)	
Absent	46 (95.8)	147 (81.7)	
Iris neovascularization			0.09
Present	2 (4.2)	23 (12.2)	
Absent	46 (95.8)	157 (87.9)	
IIRC stage [‡]			
A	0 (0.0)	0 (0.00)	1.00
B	1 (2.1)	10 (5.6)	0.47
C	10 (20.8)	30 (16.7)	0.50
D	28 (58.3)	85 (47.2)	0.17
E	9 (18.8)	55 (30.6)	0.11
Choroid invasion	n = 10	n = 38	0.28
Present	2 (20.0)	17 (44.7)	
Absent	8 (80.0)	21 (55.3)	
Optic nerve invasion	n = 10	n = 38	0.14
Present	1 (10.0)	14 (36.8)	
Absent	9 (90.0)	24 (63.2)	
Degree of differentiation	n = 10	n = 38	
Well differentiated	9 (90.0)	7 (18.4)	<0.001 [§]
Moderate	1 (10.0)	18 (47.4)	0.03 [§]
Poor	0 (0.0)	13 (34.2)	0.03 [§]

CT = computed tomography; IIRC = International Intraocular Retinoblastoma Classification; MRI = magnetic resonance imaging; RB = retinoblastoma.
*Two patients with bilateral retinoblastoma presented with cavitory lesions in both eyes, while 8 patients with bilateral retinoblastoma exhibited cavitory features in only 1 eye.

[†]According to CT or MRI presentations.

[‡]The International Intraocular Retinoblastoma Classification. Ophthalmol Clin North Am. 2005 Mar;18(1):41-53, viii.

[§]Statistical significance.

Kaplan–Meier estimates, CRB presented with more favorable outcomes in both metastasis-free survival (hazard ratio = 0.11, 95% confidence interval [0.04–0.26], log-rank $P = 0.007$, Fig 1J) and overall survival (hazard ratio = 0.15, 95% confidence interval [0.06–0.38], log-rank $P = 0.03$, Fig 1K).

Spatial Proteomic Analysis and Validation

To elucidate the molecular features of the pathological characteristics of CRB, we selected 3 primary, untreated formalin-fixed paraffin-embedded samples of CRB and compared them with 3 solid RBs lacking translucent cavities as controls (Fig 2A and Fig S2). To mitigate any potential bias, we ensured that all 6 samples (3 CRB and 3 non-CRB) were sourced from unilateral RB individuals, with

an onset age ranging from 6 to 12 months and an initial diagnosis at group D. Molecular analysis of these samples disclosed somatic *RB1* mutations across all samples examined.

Employing unbiased spatial proteomics on formalin-fixed paraffin-embedded tissue sections, we conducted an LCM procedure focused on the cancerous regions, which were delineated by the harmonized annotations of 2 board-certified pathologists (F.G. and L.M.) from the Department of Pathology at Shanghai Ninth People's Hospital. The procured samples were subsequently subjected to mass spectrometry-based proteomic analysis, yielding the quantification of a comprehensive 3514 proteins. This analysis revealed a significant differential expression profile, with 328 proteins upregulated and 422 downregulated in CRB samples (fold change >1.5 , $P < 0.05$, deposited in

Spatial Proteomic Analysis

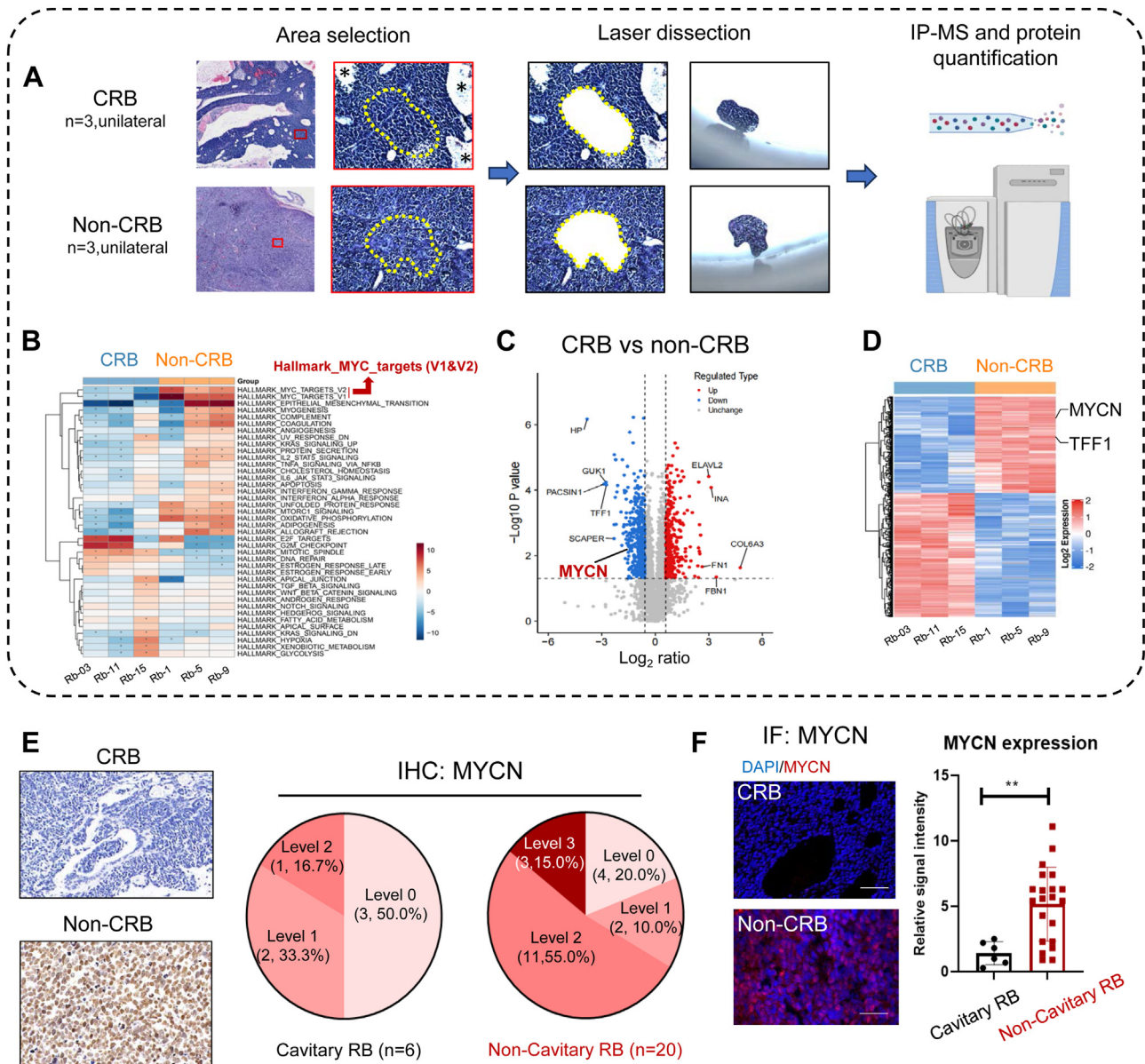


Figure 2. Downregulation of MYCN in cavitory retinoblastomas as revealed by spatial proteomic analysis. **A**, A comparative spatial proteomic map of three representative CRB and non-CRB samples, with the region of interest highlighted in red and the laser-captured microdissected area delineated by a yellow dashed circle. **B to D**, Gene set enrichment analysis (**B**) and a volcano plot (**C**) are juxtaposed with a heatmap (**D**) to illustrate the differential expression of proteins between cavitory and noncavitory tumors. **E and F**, Immunohistochemistry (**E**) and IF (**F**) are utilized to assess MYCN expression levels in RB samples, categorized into the CRB group (n = 6) and the noncavitory group (n = 20). Statistical significance is denoted by **, indicating $P < 0.01$. CRB = cavitory retinoblastoma; DAPI = 4',6-diamidino-2-phenylindole; IF = immunofluorescence; IHC = immunohistochemistry; IP-MS = immunoprecipitation-mass spectrometry; MYC = myelocytomatosis oncogene; RB = retinoblastoma; TFF1 = trefoil factor 1.

NODE database, <https://www.biosino.org/>, accession number: OEP005451, Fig 2B, C).

In a compelling revelation, single sample gene set enrichment analysis of our spatial proteomic data has underscored that myelocytomatosis oncogene-associated pathways are the most significantly downregulated hallmark pathway in CRB (according to MSigDB Hallmark gene set,¹⁷ Fig 2B, Fig S3A, and Table S2, available at www.ophtalmologyscience.org).

This finding is congruent with the previously characterized dichotomy in RB molecular patterns based on myelocytomatosis oncogene-signaling status.²² In corroboration, MYCN exhibited a pronounced reduction in expression within CRB tumors, while other members of the myelocytomatosis oncogene family maintained their expression levels. Additionally, trefoil factor 1, known for its high abundance in MYCN-expressing RBs as per

previous reports,²² was found to be consistently diminished in CRB samples (Fig 2D, Fig S3B).

Extending our investigation to an expanded sample cohort ($n = 6$ for CRB and $n = 20$ for the non-CRB group), we consistently observed a more restrained presence of MYCN signals in CRB samples relative to non-CRB groups, as demonstrated by both immunohistochemistry (Fig 2E) and immunofluorescence (Fig 2F) assays. These collective observations underscore the attenuated MYCN signaling as a pivotal molecular shift in the etiology of CRB.

Abrogation of MYCN Recapitulates Cavitory Phenotypes in RB

Considering that CRB represents a low-risk clinical subtype characterized by diminished MYCN expression, we were intrigued by the possibility that artificially reducing MYCN in RB with an abundance of MYCN could potentially induce the phenotypic traits associated with CRB formation. To test this hypothesis, we have initially established patient-derived xenograft from an MYCN-amplified RB patient (deposited in genome-wide association studies analysis, accession number: OEP005189, Fig S4, available at www.opthalmologyscience.org), and we have designed AAV2-carrying short hairpin RNAs of MYCN for the intraocular delivery of RB as we previously reported²⁰ (Fig 3A). The delivery of AAV2-mediated MYCN silencing exhibits remarkable silencing efficacy, as validated in both quantitative reverse transcription polymerase chain reaction (Fig 3B), western blot (Fig 3C), and immunofluorescence analysis (Fig 3D).

Importantly, the exogenous inhibition of MYCN leads to increased translucent cavities in the MYCN-amplified patient-derived xenografts ($P < 0.01$, Fig 3E, F), with increased numbers of cone-like rosettes (Fig 3G). The control group did not show the formation of translucent cavities with undifferentiated status. This observation agrees with our clinical finding that all CRBs are well-differentiated. Furthermore, according to previous high-throughput transcriptome analyses conducted on a cohort of 76 RB patients (GEO database: GSE59983),²³ we observed a consistent negative correlation between MYCN and the mature-cone precursor marker ARR3 ($R = -0.431$, $P < 0.0001$, Fig 3H). These findings collectively suggest that the reduction of MYCN is a fundamental molecular mechanism underlying the development of CRB. This is consistent with the notion that CRB is typified by the presence of cone-like rosettes and that MYCN overexpression is indicative of a high-risk and undifferentiated RB subtype.^{22,24–27}

Discussion

It is widely recognized that CRB constitutes a more indolent variant of RB; however, the molecular features of this subtype remain largely obscure. In this study, we have established the largest CRB cohort and demonstrated that cavity RB exhibits favorable outcomes in both metastasis-free survival and overall survival in a case-control cohort

design. Additionally, we have identified a decreased MYCN expression close to the cavitory locus, with enhanced photoreceptor-like differentiation. This downregulation is associated with the development of translucent cavities and an enhanced formation of cone-like differentiation rosettes within the tumor microenvironment. Our findings delineate a novel genetic–phenotypic link, underscoring the pivotal role of MYCN in driving cellular differentiation pathways and influencing the clinical outcomes in RB (Fig 3I).

The hallmark of CRB is the presence of translucent intratumoral cavities that are discernible upon ophthalmoscopy. These cavities characteristically exhibit hypofluorescence on fluorescein angiography and appear echolucent on B-scan ultrasonography. While certain studies have suggested an infrequent association between CRB and vitreous seeds, others have reported a more variable correlation, indicating that the presence of vitreous seeds is not a uniform characteristic.^{4,7,9} In this study, CRBs demonstrated a lower prevalence of vitreous seeds, consistent with their generally less aggressive behavior. As aqueous humor could serve as a liquid biopsy with diagnostic and prognostic value for RB,²⁸ it is insightful to explore the aqueous humor characteristics specific to CRB in the future study.

Furthermore, CRB tumors are noted for their stability in dimensions over time, often lacking the significant regression or progression observed in more aggressive RB variants.⁸ Owing to their higher degree of differentiation, CRBs may respond less markedly to chemotherapy, potentially showing minimal flattening or calcification posttreatment.⁹ This observation supports a more conservative therapeutic strategy.²⁹ Our study revealed that patients treated with a combination of intra-arterial and IVC achieved a full response rate of 100%. This finding may indicate the efficacy of this combined chemotherapeutic approach in the management of CRB.

The MYCN oncogene, while amplified in only approximately 1% to 9% of RB tumors, stands out as a significant genetic aberration in this disease, second only to mutations in the RB1 gene.²⁴ Beyond genetic amplification, MYCN is observed to be upregulated at both RNA and protein levels, with its overexpression being a notable feature in >60% of RB tumor samples, even in MYCN normal copy number tumors.³⁰ Importantly, MYCN overexpression is distinguished by its less differentiated cone states and the expression of genes characteristic of neuronal or ganglion cell lineages, suggesting a potential stem-like or progenitor cell origin.^{24,25,31,32} This notion is in alignment with our observation that MYCN downregulation could further promote the differentiation of cone precursors, representing a low-risk molecular subtype. Notably, it would be valuable to investigate the proteomic pattern in patients with retinocytoma in future studies. This could establish a comprehensive genotype–phenotype spectrum ranging from retinocytoma, through CRB, to poorly differentiated RB.

The hallmark magnetic resonance imaging features of MYCN amplification provide a diagnostic inroad, characterized by a peripheral tumor location, a distinct placoid configuration, retinal folding, hemorrhage-associated with the tumor, and anterior chamber enhancement.³³ Our

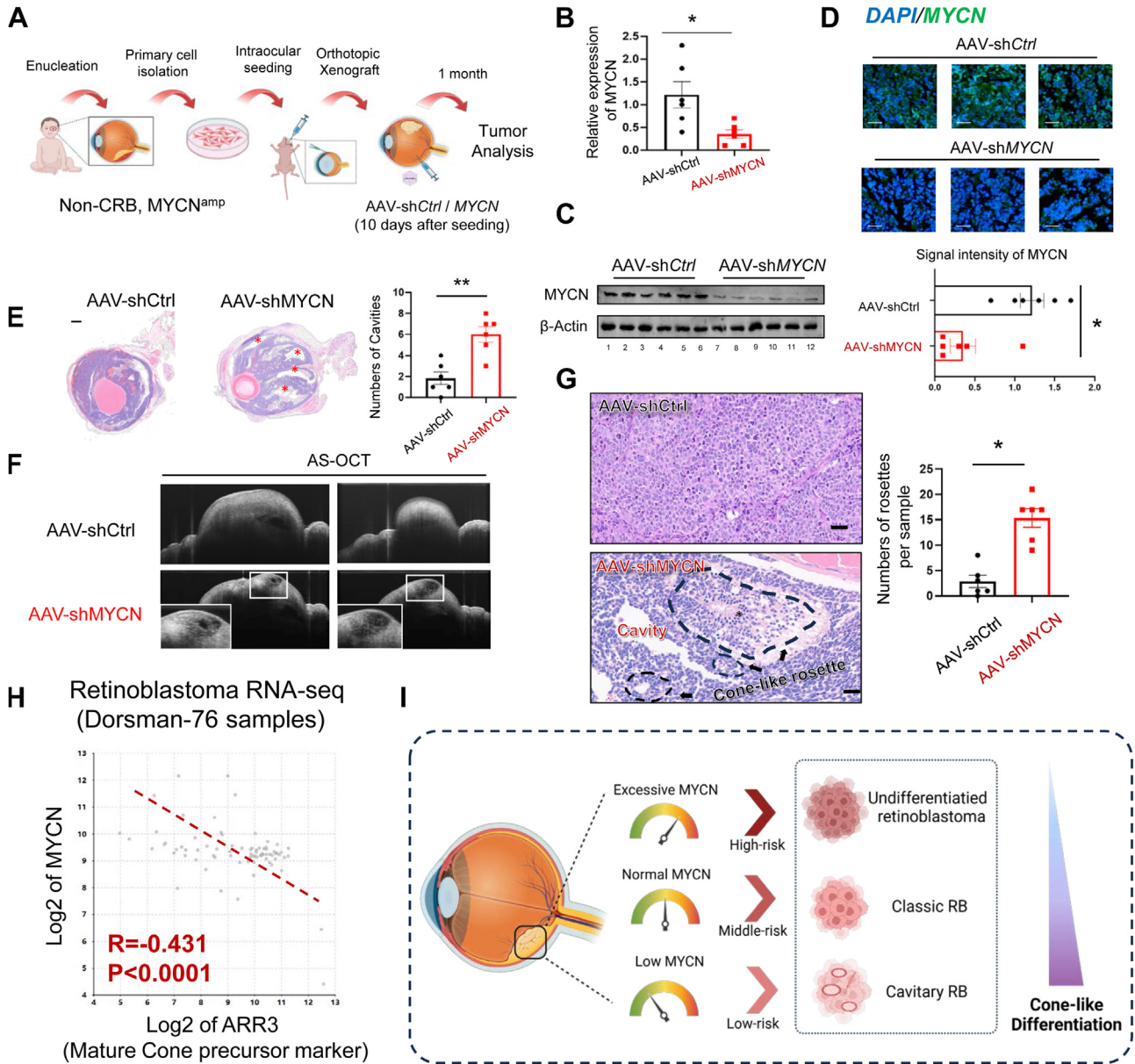


Figure 3. MYCN suppression recapitulates the phenotypic characteristics of CRB in PDXs. **A**, A schematic representation of the experimental design for MYCN knockdown using AAV2-mediated gene silencing in a PDX model with MYCN amplification. **B to D**, Assessment of MYCN knockdown efficacy through quantitative PCR (**B**), western blot (**C**), and immunofluorescence analysis (**D**) in the treated PDXs (n = 6 per group). Statistical significance is indicated by *, representing $P < 0.05$. **E**, A pathological examination documenting the number of cavities formed in MYCN-silenced PDXs. **F**, Anterior segment OCT imaging of the cavitory structures in MYCN-silenced PDXs compared with the control group. **G**, Pathological evaluation of the phenotypic changes induced by AAV2-shMYCN in MYCN-amplified PDXs. Scale bar: 10 μ m. **H**, A correlation analysis linking MYCN expression with ARR3 across a comprehensive dataset of 76 RB samples. The data are created in R2 Genomics Analysis and Visualization Platform (<https://hgserver1.amc.nl/>), by using genome-wide mRNA expression profiling data in the 76 RB samples (GEO: GSE59983). **I**, A conceptual diagram illustrating the negative correlation between MYCN expression and differentiation status, with reduced MYCN levels implicated in the development of cavitory features. AAV = adeno-associated virus; AS-OCT = anterior segment OCT; CRB = cavitory retinoblastoma; DAPI = 4',6-diamidino-2-phenylindole; PCR = polymerase chain reaction; PDX = patient-derived xenograft; RB = retinoblastoma.

investigation within the subset of CRB samples revealed a profound decrease in MYCN expression. Utilizing AAV2-mediated targeted ablation of MYCN, our study has uncovered a significant therapeutic response, suggesting a strategy that may steer RB toward a more differentiated and

less aggressive phenotype. Consequently, the targeted approach toward MYCN ablation emerges as a promising therapeutic avenue, particularly for undifferentiated RBs.

Notably, although most CRBs have favorable outcomes, 1 CRB case developed brain metastasis and death. This is a

case of bilateral RB, with the left eye classified as group E and the right eye as group C. The left eye displayed typical cavitory characteristics, while the right eye did not. The left eye of the patient was initially enucleated, after 2 cycles of IVC. However, the parents declined further chemotherapy. Two years later, the patient was diagnosed with brain metastasis and passed away 10 months after this diagnosis. This outcome suggests that, despite typically being considered a low-risk subtype, standardized chemotherapy remains crucial for effective tumor management in CRB cases.

To our knowledge, this is the largest multicentric cohort of CRB, revealing a significantly lower metastatic rate and favorable overall survival of this subtype. Furthermore, we establish a novel genetic–phenotypic association, highlighting the critical function of MYCN in modulating cellular differentiation processes and its impact on the clinical prognosis of RB. Therapeutically, the targeted silencing of MYCN presents as a potentially efficacious therapeutic strategy, particularly for high-risk, undifferentiated RBs characterized by overexpression of MYCN. This approach

may pave the way for more personalized and effective treatment options for patients afflicted with this aggressive form of RB.

Data Sharing Statement

The spatial proteomic analysis was deposited in the National Omics Data Encyclopedia (NODE), <https://www.biosino.org/>, accession number: OEP005451. The genotyping of relevant patients was determined by genome-wide association studies, deposited in NODE, accession number OEP005189. The correlation analysis was created in R2 Genomics Analysis and Visualization Platform (<https://hgserver1.amc.nl/>), by using genome-wide mRNA expression profiling data in the 76 RB samples (GEO: GSE59983).

Acknowledgments

The authors thank Prof. Maurizio Tonetti for his kind assistance in the revision.

Footnotes and Disclosures

Originally received: October 19, 2024.

Final revision: April 24, 2025.

Accepted: April 25, 2025.

Available online: May 6, 2025. Manuscript no. XOPS-D-24-00450.

¹ Department of Ophthalmology, Xinhua Hospital, Shanghai Jiao Tong University School of Medicine, Shanghai, People's Republic of China.

² Department of Ophthalmology, Ninth People's Hospital, Shanghai Jiao Tong University School of Medicine, Shanghai, People's Republic of China.

³ State Key Laboratory of Eye Health, Shanghai Key Laboratory of Orbital Diseases and Ocular Oncology, Shanghai, People's Republic of China.

*M.X., H.S., Y.S., and L.Y. contributed equally to this manuscript.

Disclosure(s):

All authors have completed and submitted the ICMJE disclosures form.

The author(s) have no proprietary or commercial interest in any materials discussed in this article.

This work was supported by grants from the National Natural Science Foundation of China (82373298 and 82103240), the Science and Technology Commission of Shanghai (23ZR1480100), the Project of Biobank of Shanghai Ninth People's Hospital, Shanghai Jiao Tong University School of Medicine (YBKA201907, YBKA202208), and the Innovative Research Team of High-Level Local Universities in Shanghai, Shanghai Municipal Health Commission (GWVI-11.2-YQ19). The funders did not participate in any aspect of the study, including its design, execution, analysis, data collection, interpretation, peer review, or the decision to submit the work for publication.

HUMAN SUBJECTS: Human subjects were included in this study. A centralized institutional review board review process was used in this study. This study was approved by the institutional review board of the lead unit, Shanghai Ninth People's Hospital, Shanghai Jiao Tong University School of Medicine (identifier, 2017-353-246 T262, SH9H-2019-T185-2). All research adhered to the tenets of the Declaration of Helsinki. All participants provided informed consent.

ANIMAL SUBJECTS: Animal subjects were used in this study. The animal studies were granted approval by the Animal Ethics Committee of Shanghai Jiao Tong University School of Medicine, with the reference number SH9H-

2021-A058-SB and were conducted in strict adherence to the prevailing institutional and international standards for the welfare and utilization of animals. BALB/c nude mice, aged four weeks, were procured from Slack Company (Shanghai, China), and were housed in the hospital's specific pathogen-free Laboratory Animal Facility.

Author Contributions:

Conception and design: Jia, Han, Fan, Chai

Data collection: Xu, Shi, Shen, Yang, Luan, Gu, Wen, Jia, Ji, Zhao, Han, Fan, Chai

Analysis and interpretation: Xu, Shi, Shen, Yang, Luan, Wen, Zhou, Jia, Ji, Zhao, Han, Fan, Chai

Obtained funding: Fan, Chai

Overall responsibility: Xu, Shi, Shen, Yang, Luan, Gu, Wen, Zhou, Jia, Ji, Zhao, Han, Fan, Chai

Abbreviations and Acronyms:

AAV = adeno-associated virus; **CRB** = cavitory retinoblastoma; **EtOH** = ethanol; **IVC** = intravenous chemotherapy; **LCM** = laser-capture microdissection; **MS** = mass spectrum; **RB** = retinoblastoma.

Keywords:

Cavitory retinoblastoma, MYCN, Cone-like differentiation.

Correspondence:

Peiwei Chai, MD, PhD, Department of Ophthalmology, Ninth People's Hospital, Shanghai Jiao Tong University School of Medicine, Shanghai 200011, People's Republic of China. E-mail: chaipeiwei123@sjtu.edu.cn; and Jiayan Fan, MD, PhD, Department of Ophthalmology, Ninth People's Hospital, Shanghai Jiao Tong University School of Medicine, Shanghai 200011, People's Republic of China. E-mail: fanjiayan1118@126.com; and Minglei Han, MD, PhD, Department of Ophthalmology, Ninth People's Hospital, Shanghai Jiao Tong University School of Medicine, Shanghai 200011, People's Republic of China. E-mail: hanminglei222@126.com; and Peiquan Zhao, MD, PhD, Department of Ophthalmology, Xinhua Hospital, Shanghai Jiao Tong University School of Medicine, Shanghai 200011, People's Republic of China. E-mail: zhaopeiquan@126.com; and Xunda Ji, MD, PhD, Department of Ophthalmology, Xinhua Hospital, Shanghai Jiao Tong University School of Medicine, Shanghai 200011, People's Republic of China. E-mail: jixunda@xinhua.com.cn.

References

- Zhou C, Wen X, Ding Y, et al. Eye-preserving therapies for advanced retinoblastoma: a multicenter cohort of 1678 patients in China. *Ophthalmology*. 2022;129:209–219.
- Larkin HD. Retinoblastoma especially deadly in children in low-income countries. *JAMA*. 2022;328:611.
- Wen X, Fan J, Jin M, et al. Intravenous versus super-selected intra-arterial chemotherapy in children with advanced unilateral retinoblastoma: an open-label, multi-centre, randomised trial. *Lancet Child Adolesc Health*. 2023;7:613–620.
- Mashayekhi A, Shields CL, Eagle Jr RC, Shields JA. Cavitory changes in retinoblastoma: relationship to chemoresistance. *Ophthalmology*. 2005;112:1145–1150.
- Palamar M, Pirondini C, Shields CL, Shields JA. Cavitory retinoblastoma: ultrasonographic and fluorescein angiographic findings in 3 cases. *Arch Ophthalmol*. 2008;126:1598–1600.
- Yi X, Lin X, Fang C, et al. Assessment of retinal microvasculature and choroidal vascularity after intra-arterial chemotherapy for retinoblastoma. *Am J Ophthalmol*. 2024;266:10–16.
- Rojanaporn D, Kaliki S, Bianciotto CG, et al. Intravenous chemoreduction or intra-arterial chemotherapy for cavitory retinoblastoma: long-term results. *Arch Ophthalmol*. 2012;130:585–590.
- Chaudhry S, Onadim Z, Sagoo MS, Reddy MA. The recognition of cavitory retinoblastoma tumors: implications for management and genetic analysis. *Retina*. 2018;38:782–787.
- Rishi P, Sharma U, Sharma T. Cavitory retinoblastoma: clinical observations. *Eye (Lond)*. 2020;34:704–710.
- Linn Murphree A. Intraocular retinoblastoma: the case for a new group classification. *Ophthalmol Clin North Am*. 2005;18:41–53. viii.
- Eisenhauer EA, Therasse P, Bogaerts J, et al. New response evaluation criteria in solid tumours: revised RECIST guideline (version 1.1). *Eur J Cancer*. 2009;45:228–247.
- Alkatan HM, AlQahtani FS, Maktabi AM. Enucleated globes with advanced retinoblastoma: correlation of histopathological features and reclassification of tumors according to the 8th edition of the American Joint Committee on Cancer (AJCC). *Int Ophthalmol*. 2020;40:1739–1747.
- Shi H, Tian H, Zhu T, et al. Single-cell sequencing depicts tumor architecture and empowers clinical decision in metastatic conjunctival melanoma. *Cell Discov*. 2024;10:63.
- Ying W. Phenomic studies on diseases: potential and challenges. *Phenomics*. 2023;3:285–299.
- Yu J, Zhuang A, Gu X, et al. Nuclear PD-L1 promotes EGR1-mediated angiogenesis and accelerates tumorigenesis. *Cell Discov*. 2023;9:33.
- Gu X, Zhuang A, Yu J, et al. Histone lactylation-boosted ALKBH3 potentiates tumor progression and diminished promyelocytic leukemia protein nuclear condensates by m1A demethylation of SP100A. *Nucleic Acids Res*. 2024;52:2273–2289.
- Liberzon A, Birger C, Thorvaldsdóttir H, et al. The Molecular Signatures Database (MSigDB) hallmark gene set collection. *Cell Syst*. 2015;1:417–425.
- Lv J, Wang H, Cheng X, et al. AAV1-hOTOF gene therapy for autosomal recessive deafness 9: a single-arm trial. *Lancet*. 2024;403:2317–2325.
- Puissant A, Frumm SM, Alexe G, et al. Targeting MYCN in neuroblastoma by BET bromodomain inhibition. *Cancer Discov*. 2013;3:308–323.
- Shi H, He X, Yang Z, et al. The use of rAAV2-RB1-mediated gene therapy in retinoblastoma. *Invest Ophthalmol Vis Sci*. 2023;64:31.
- Fuller TS, Alvi RA, Shields CL. Optical coherence tomography of cavitory retinoblastoma. *JAMA Ophthalmol*. 2016;134:e155355.
- Liu J, Ottaviani D, Sefta M, et al. A high-risk retinoblastoma subtype with stemness features, dedifferentiated cone states and neuronal/ganglion cell gene expression. *Nat Commun*. 2021;12:5578.
- Kooi IE, Mol BM, Moll AC, et al. Loss of photoreceptor and gain of genomic alterations in retinoblastoma reveal tumor progression. *EBioMedicine*. 2015;2:660–670.
- Felsher DW. Role of MYCN in retinoblastoma. *Lancet Oncol*. 2013;14:270–271.
- Wu N, Jia D, Bates B, et al. A mouse model of MYCN-driven retinoblastoma reveals MYCN-independent tumor reemergence. *J Clin Invest*. 2017;127:888–898.
- Blixt MKE, Hellsand M, Konjusha D, et al. MYCN induces cell-specific tumorigenic growth in RB1-proficient human retinal organoid and chicken retina models of retinoblastoma. *Oncogenesis*. 2022;11:34.
- Zhang H, Konjusha D, Rafati N, et al. Inhibition of high level E2F in a RB1 proficient MYCN overexpressing chicken retinoblastoma model normalizes neoplastic behaviour. *Cell Oncol (Dordr)*. 2024;47:209–227.
- Berry JL, Pike S, Shah R, et al. Aqueous humor liquid biopsy as a companion diagnostic for retinoblastoma: implications for diagnosis, prognosis, and therapeutic options: five years of progress. *Am J Ophthalmol*. 2024;263:188–205.
- Raval V, Kaliki S. Cavitory retinoblastoma: a review of literature. *Surv Ophthalmol*. 2022;67:723–728.
- Sradhanjali S, Rout P, Tripathy D, et al. The oncogene MYCN modulates glycolytic and invasive genes to enhance cell viability and migration in human retinoblastoma. *Cancers (Basel)*. 2021;13.
- Qi DL, Cobrinik D. MDM2 but not MDM4 promotes retinoblastoma cell proliferation through p53-independent regulation of MYCN translation. *Oncogene*. 2017;36:1760–1769.
- Vempuluru VS, Maniar A, Bakal K, Kaliki S. Role of MYCN in retinoblastoma: a review of current literature. *Surv Ophthalmol*. 2024;69:697–706.
- Jansen RW, de Bloeme CM, Cardoen L, et al. MRI features for identifying MYCN-amplified RB1 wild-type retinoblastoma. *Radiology*. 2023;307:e222264.